

Table of Contents

List of Figures	xii
List of Tables	xviii
List of Abbreviations	xix
Abstract	xx
Chapter 1	1
Introduction	1
1.1 Hydrogen Energy	1
1.2 Hydrogen Production Processes.....	2
1.2.1 Renewable Production Methods.....	2
1.2.2 Steam Reforming Mechanisms.....	4
1.3 Catalysts for steam methane reforming.....	7
1.3.1 Literature review of steam methane reforming catalysts.....	8
1.4 Membrane Reformers.....	17
1.5 Motivation of study	25
1.6 Objectives.....	26
1.7 Structure of thesis.....	27
References.....	30
Chapter 2	41
Catalyst Preparation Methods, Characterization Techniques and Experimental Framework	41
2.1 Introduction to Catalysts	41
2.2 Catalyst Preparation Methods	41
2.2.1 Impregnation Method	42
2.2.2 Precipitation Method	43
2.2.3 Co-precipitation Method.....	43
2.2.4 Sol-Gel Method	44
2.2.5 Chemical Vapor Deposition (CVD).....	45
2.2.6 Atomic Layer Deposition (ALD).....	45

2.3. Characterization Techniques for Catalysts	46
2.3.1 X-ray Diffraction (XRD)	46
2.3.2 Scanning Electron Microscopy (SEM).....	48
2.3.3 Transmission Electron Microscopy (TEM)	48
2.3.4 X-ray Photoelectron Spectroscopy (XPS)	50
2.3.5 Brunauer-Emmett-Teller (BET) Surface Area Analysis	51
2.3.6 FTIR Spectroscopy	52
2.4. Experimental Framework.....	53
2.4.1 Catalyst Preparation.....	54
2.4.2 Catalyst evaluation	58
2.4.3 Gas Chromatography (GC).....	58
References	62
Chapter 3	67
Monometallic Catalyst: Performance and Shape Morphology Effect	67
3.1 Monometallic Catalysts for steam methane reforming	67
3.1.1 Nickel Catalysts on Alumina Support	67
3.1.2 Nickel Catalysts on Ceria Support.....	68
3.1.3 Key literature review on Ni based monometallic catalyst.....	69
3.2 Preparation of monometallic catalysts	72
3.3 Results and discussion.....	73
3.3.1 SEM	73
3.3.2 XRD.....	74
3.3.3 BET.....	76
3.3.4 Activity Results.....	79
3.4 Summary	85
3.5 Effect of Shape morphology on Ceria.....	85
3.5.1 Literature review on shape morphology of ceria.....	86
3.5.2 Catalyst characterization.....	89
3.5.3 Catalyst synthesis procedure	90
3.5.4 Catalyst performance in packed bed reactor.....	90
3.6 Results and discussion.....	91

3.6.1 BET and XRD	91
3.6.2 TEM/EDX Results.....	96
3.6.3 Experimental results	100
3.6.4 Comparison with commercial ceria.....	102
3.7 Conclusions.....	104
References.....	106
Chapter 4	113
Role of Bimetallic Catalysts in Steam Methane Reforming.....	113
4.1 Introduction	113
4.2 Experimental analysis	114
4.2.1 Materials	114
4.2.2 Catalyst Synthesis.....	114
4.2.3 Catalyst Characterization.....	115
4.3 Catalyst Testing	116
4.4 Results and Discussion.....	117
4.4.1 Characterization results	117
4.4.2 Catalyst Activity Testing.....	123
4.5 Cobalt based bimetallic catalysts:	131
4.5.1 Alumina Supports	131
4.5.2 Cerium Oxide	131
4.6 Conclusions	133
References.....	136
Chapter 5	143
Role of Trimetallic Catalysts in Steam Methane Reforming	143
5.1 Role of trimetallic catalyst Ni-Fe-La/Al ₂ O ₃	143
5.1.1 Introduction	143
5.2 Experimental	147
5.2.1 Catalyst preparation.....	147
5.2.2 Catalyst characterization.....	147
5.2.3 Catalyst Test.....	148
5.3 Results and discussion.....	149

5.3.1 Catalytic Activity	149
5.3.2 Long term stability test	157
5.3.3 Characterization results	158
5.4 Conclusions	169
5.5 Cobalt based trimetallic catalyst Ni-Co-La/Al ₂ O ₃	170
5.5.1 Introduction	170
5.5.2 Methodology.....	174
5.5.3 Catalyst characterization.....	174
5.5.4 Catalyst testing	176
5.6 Results and discussion.....	178
5.6.1 Characterization results	178
5.6.2 Catalytic activity of steam methane reforming.....	193
5.7 Comparison of trimetallic catalysts to be used for upscaling.....	198
5.8 Conclusions	199
References.....	201
Chapter 6	211
Large scale studies of steam methane reforming in packed bed reactor.....	211
6.1 Introduction	211
6.2 Experimental section.....	212
6.2.1 Catalyst Preparation.....	212
6.2.2 Catalyst testing in packed bed reactor	212
6.3 Results and Discussion.....	216
6.3.1 Effect of temperatures	216
6.3.2 Effect of various W/F in large reactor	218
6.4 Large scale studies to 3kW.....	220
6.5 Effect of pressure	223
6.6 Characterization results	224
6.7 Conclusions	229
References.....	230
Chapter 7	235
Conclusions and Recommendations.....	235

7.1 Conclusions of study	235
7.2 Recommendations and future perspectives	240
Appendix-A.....	243
Effect of Mixed Supports.....	243
A1. Introduction	245
A2. Methodology	246
A3. Catalyst Preparation	249
A4. Catalyst Characterization	250
A5. Catalyst Activity.....	250
A6. Results and discussion	252
A7. Comparative analysis of mixed support with only alumina.....	255
A8. Characterization results.....	259
A9. Conclusions.....	262
References.....	263

LIST OF FIGURES

Fig 1.1 Qualitative percentage distribution of different catalyst used for steam methane reforming in literature.....	8
Fig 1.2 Membrane reformer technology for hydrogen production via steam methane reforming.....	18
Fig 2.1 Flow chart for synthesis of catalysts.....	57
Fig 2.2 Schematic diagram of packed bed reactor of internal diameter 11.74mm.....	59
Fig 2.3 Scale up reactor of internal diameter 6.35cm.....	60
Fig 3.1 Wet impregnation method for monometallic catalysts.....	73
Fig 3.2 SEM images of monometallic ceria and alumina supported catalysts.....	74
Fig 3.3 XRD graph of monometallic catalysts.....	76
Fig 3.4 BET graphs of monometallic catalysts (a) alumina supported (b) ceria supported.....	77
Fig 3.5 Conversion vs time graph of monometallic alumina supported catalysts.....	80
Fig 3.6 Conversion vs time graph of monometallic ceria supported catalysts.....	81
Fig 3.7 CO selectivity vs time of monometallic alumina supported catalysts.....	82
Fig 3.8 CO selectivity vs time graph of monometallic ceria supported catalysts.....	83
Fig 3.9 CO ₂ selectivity vs time graph of (a) monometallic alumina supported (b) monometallic ceria supported.....	84
Fig 3.10 Brunauer–Emmett–Teller (BET) N ₂ adsorption desorption isotherm of Ni-doped ceria nanorod and nanocube calcined at 550°C.....	92
Fig 3.11 X-ray diffraction (XRD) analysis of Ni doped ceria (a) nanorod calcined at 550°C,	

(b) nanorod calcined at 970°C, (c) nanocube calcined at 550°C, and (d) nanocube calcined at 970°C.....95

Fig 3.12: Transmission electron microscopy (TEM) image of Ni-doped ceria support. (a) Nanorod calcined at 550°C, (b) nanocube calcined at 550°C, (c) nanorod calcined at 970°C, (d) nanocube calcined at 970°C, (e) spent nanorod catalyst calcined at 550°C and reduced at 850°C, and (f) spent nanocube calcined at 550°C reduced at 850°C.....98

Fig 3.13 EDX analysis of (a) Ni-doped nano cube calcined at 550°C and (b) Ni-doped nano rod calcined at 550°C as received and as implanted.....100

Fig 3.14 Conversion versus time graph of (a) nanorod calcined at 550°C and (b) nanocube calcined at 550°C.....101

Fig 3.15 CO selectivity vs time graph for (a) nanorod calcined at 550°C (b) nanocube calcined at 550°C, CO₂ selectivity (c) nanorod calcined at 550°C (d) nanocube calcined at 550°C.....102

Fig 3.16 Comparison of commercial ceria with shapes (a) conversion graph of samples calcined at 550°C (b) conversion graph of samples calcined at 970°C (c) CO selectivity graph of samples calcined at 550°C (d) CO selectivity graph of samples calcined at 970°C.....104

Fig 4.1. XRD graph of La and Fe doped bimetallic catalysts.....118

Fig 4.2. BET Analysis of Ni/CeO₂, Ni-La/CeO₂, Ni-Fe/CeO₂.....121

Fig 4.3. SEM images of a) Ni/Al₂O₃, b) Ni-La/Al₂O₃, c) Ni-Fe/Al₂O₃, d) Ni/CeO₂, e) Ni-La/CeO₂, and f) Ni-Fe/CeO₂123

Fig 4.4. a) EDS mapping of Ni-La/Al₂O₃, b) Ni-La/CeO₂.....123

Fig 4.5. Conversion vs temperature plots for a) Ni/Al₂O₃, Ni-La/Al₂O₃, Ni-Fe/Al₂O₃, b) Ni/CeO₂, Ni La/CeO₂, Ni Fe/CeO₂ (reaction conditions: P = 1 atm, H₂O/ CH₄ = 4.0, W/F= 26.8 Kg_{cat}.s/mol).....126

Fig 4.6. Conversion vs time graph for a) Ni-Fe/Al ₂ O ₃ , b) Ni-La/Al ₂ O ₃ c) Ni-Fe/CeO ₂ d) Ni-La/CeO ₂ catalysts at different temperatures.....	128
Fig 4.7. CO selectivity with temperature for a) alumina supported b) ceria supported catalysts.....	128
Fig 4.8. CO ₂ selectivity with temperature for a) alumina supported b) ceria supported catalysts.....	129
Fig 4.9. Conversion vs time graph of (a) alumina supported catalysts (b) ceria supported catalysts.....	131
Fig 4.10. Catalyst activity of Ni-Co/Al ₂ O ₃ catalyst (a) Methane conversion vs time (b) CO selectivity vs time (c) CO ₂ selectivity vs time graph.....	132
Fig 5.1 (a) Conversion vs Temperature graph of different compositions (b) conversion vs time graph 75Ni-20Fe-5La (c) conversion vs time graph of 75Ni-15Fe-10La (d) conversion vs time graph of 75Ni-10Fe-10La.....	151
Fig 5.2 Catalytic activity of 75Ni-15Fe-10La (a) Conversion vs time (b) H ₂ yield vs time (c) CO selectivity vs time (d) CO ₂ selectivity vs time.....	152
Fig 5.3 Effect of W/F on 75Ni-15Fe-10La at 700 °C (a) Conversion vs time graph (b) H ₂ Yield vs time (c) CO selectivity vs time (d) CO ₂ selectivity vs time.....	153
Fig 5.4 Conversion, H ₂ production rate vs W/F value for 75Ni-15Fe-10La catalyst at 700 °C...154	
Fig 5.5 (a) Conversion vs metal loading graph of 75Ni-15Fe-10La catalyst (b) Conversion vs time graph w.r.t metal loadings (c) CO ₂ selectivity vs time graph (d) H ₂ yield vs time graph.....	155
Fig 5.6 Long term stability test of 75Ni-15Fe-10La catalyst for at least 130 hours.....	156
Fig 5.7 SEM images of (a) Fresh 75Ni-10Fe-15La (b) Fresh 75Ni-15Fe-10La (c) spent 75Ni-10Fe-15La (d) 75Ni-15Fe-10La.....	158

Fig 5.8. EDS analysis of catalysts (a) Fresh 75Ni-10Fe-15La (b) Spent 75Ni-10Fe-15La (c) Fresh 75Ni-15Fe-10La (d) Spent 75Ni-15Fe-10La.....	158
Fig 5.9 XRD graphs of fresh and spent trimetallic catalysts.....	162
Fig 5.10 XPS spectra Ni-Fe-La/Al ₂ O ₃ catalyst.....	164
Fig 5.11 FTIR spectra of fresh and spent 75Ni-15Fe-10La catalyst.....	165
Fig 5.12 TEM analysis of (a) Fresh 75Ni-15Fe-10La (b) SAED pattern of fresh catalyst (c) Average particle size of fresh catalyst (d) Spent 75Ni-15Fe-10La (e) SAED pattern of spent catalyst (f) Interplanar distant of spent catalyst.....	167
Fig 5.13 Schematic diagram of catalytic reformer.....	176
Fig 5.14 XRD graph of alumina and ceria supported catalysts.....	178
Fig 5.15 Adsorption-desorption isotherm of (a) ceria supported (b) alumina supported catalysts.....	180
Fig 5.16 SEM images of a) La/CeO ₂ , b) Co/CeO ₂ , c) Ni-Co/CeO ₂ , d) Co-La/CeO ₂ , e) La/Al ₂ O ₃ , f) Co/Al ₂ O ₃ , g) Ni-Co/Al ₂ O ₃ , h) Co-La/Al ₂ O ₃ (i) Ni-Co-La/Al ₂ O ₃ (j) Ni-Co-Fe/Al ₂ O ₃ (k) Spent Ni-Co-La/Al ₂ O ₃ (l) Spent Ni-Co-Fe/Al ₂ O ₃	183
Fig 5.17 EDS images (a) Spent Ni-Co-La/Al ₂ O ₃ and d) Spent Ni-Co-Fe/ Al ₂ O ₃	185
Fig 5.18 TEM images of a) Ni-Co/Al ₂ O ₃ , b) Ni-Co-Fe/Al ₂ O ₃ , c) Ni-Co-La/Al ₂ O ₃ d) Spent Ni-Co-La/Al ₂ O ₃ and e) Spent Ni-Co- Fe/Al ₂ O ₃	186
Fig 5.19 FTIR analysis of synthesized catalysts.....	189
Fig 5.20 (a) conversion vs temperature graph of all alumina supported catalysts (b) CO selectivity vs temperature graph (c) CO ₂ selectivity vs temperature graph (d) Conversion vs temperature graph of both trimetallic catalysts at 700°C.....	191

Fig 5.21 Conversion, H ₂ production rate vs W/F graph of Ni-Co-La/Al ₂ O ₃ catalyst.....	192
Fig 5.22 Life cycle study of Ni-Co-La/Al ₂ O ₃ catalyst.....	193
Fig 5.23 Conversion vs time graph of Ni-Co-La/Al ₂ O ₃ at different S/M ratios.....	194
Fig 5.24 Comparison of all trimetallic catalysts (a) Conversion graph (b) CO selectivity graph (c) CO ₂ selectivity.....	195
Fig 6.1 Experimental set up of scale up reactor of I.D 6.35cm.....	211
Fig 6.2 Conversion vs time graph of Ni-Co-La/Al ₂ O ₃ catalyst for all temperatures for 1 kW system.....	213
Fig 6.3 Ni-Co-La/Al ₂ O ₃ catalyst for all temperatures for 1 kW system (a) CO selectivity (b) CO ₂ selectivity vs time.....	214
Fig 6.4 Conversion vs time graph of Ni-Co-La/Al ₂ O ₃ catalyst for W/F values.....	215
Fig 6.5 Ni-Co-La/Al ₂ O ₃ catalyst for W/F for 1 kW system (a) CO selectivity (b) CO ₂ selectivity.....	216
Fig 6.6 Conversion vs time graph of Ni-Co-La/Al ₂ O ₃ catalyst for 3kW system at 700°C.....	218
Fig 6.7 Ni-Co-La/Al ₂ O ₃ catalyst for 3kW system for CO selectivity.....	219
Fig 6.8 Conversion vs time graph of Ni-Co-La/Al ₂ O ₃ catalyst for all pressures for 1 kW system at 700°C (a) Conversion (b) CO selectivity (c) CO ₂ selectivity.....	220
Fig 6.9 TEM image of Ni-Co-La/Al ₂ O ₃ catalyst powder pellets for 1 kW system (a-c) Fresh catalyst (d-f) Spent catalyst after small reactor of I.D 11.74mm (g-i) Spent catalyst after scale up reactor of I.D 6.35cm.....	222
Fig 6.10 Ni-Co-La/Al ₂ O ₃ catalyst powder pellets for 1 kW system (a) Fresh catalyst (b) Spent catalyst after scale up reactor.....	224

Fig A1. Conversion vs time graph (a) 75Al/25Ce (b) 50Al/50Ce (c) 80Al/20Ce.....	247
Fig A2. Conversion vs time graph of 80Al/20Ce ratio for all temperatures.....	249
Fig A3. (a) CO selectivity vs time graph of 80Al/20Ce catalyst (b) CO ₂ selectivity vs time graph.....	250
Fig A4. Conversion vs time graph of mixed support and without ceria support.....	251
Fig A5. (a) CO selectivity vs time graph (b) CO ₂ selectivity vs time graph.....	252
Fig A6. Effect of W/F for Ni-Co-La/Ce-Al ₂ O ₃ catalyst.....	253
Fig A7. SEM images of (a)75Al/25Ce (b) 80Al/20Ce (c) 50Al/50Ce.....	254
Fig A8. TEM images of mixed supports(a) 80Al/20Ce (b) 75Al/25Ce (c) 50Al/50Ce.....	256

LIST OF TABLES

Table 1.1 Key Literature on steam methane reforming catalysts.....	10
Table 1.2 Key literature on membrane reformer using methane.....	19
Table 2.1 Monometallic Catalysts synthesized on alumina and ceria supports.....	56
Table 2.2 Bimetallic Catalysts synthesized on alumina and ceria supports.....	56
Table 2.3 Trimetallic Catalysts synthesized on alumina support.....	56
Table 2.4 Calibration factors used in analysis of GC results for mixture of gases.....	61
Table 3.1 Literature survey on Nickel based monometallic catalyst.....	69
Table 3.2 Surface area, pore volume, pore diameter and crystallite size for monometallic alumina supported catalysts.....	79
Table 3.3 Catalyst shape morphology effect on steam reforming.....	87
Table 3.4 BET surface area, pore volume and pore diameter of different catalysts.....	94
Table 3.5 Crystallite sizes of various ceria shape morphologies.....	97
Table 4.1. Composition of prepared catalysts.....	115
Table 4.2. BET surface area analysis of synthesized catalysts.....	121
Table 4.3. Elemental composition of catalysts through EDS analysis.....	122
Table 5.1 Literature survey.....	144
Table 5.2 BET surface area, pore volume and pore diameter of catalysts.....	160
Table 5.3 Literature survey.....	171
Table 5.4 BET analysis of all the catalysts.....	180
Table 6.1 Specifications for small and scale up reactor.....	211
Table 6.2 BET surface area, pore volume, pore diameter and type of isotherm of catalysts.....	223
Table A1. Literature survey.....	241

List of abbreviations

SMR	Steam methane reforming
MR	Membrane reformer
GC	Gas chromatography
PEMFC	Proton exchange membrane fuel cell
XRD	X-ray diffraction
BET	Brunauer-Emmett-Teller
SEM	Scanning electron microscope
EDS	Energy dispersive X-ray spectroscopy
TEM	Transmission electron microscope
XPS	X-ray photoelectron spectroscopy
FTIR	Fourier transform infrared spectroscopy

Appendix-A

Effect of Mixed Supports

Abstract

The development of efficient and stable catalysts for steam methane reforming (SMR) is crucial for hydrogen production. In this study, a series of Ni-Co-La catalysts supported on mixed Al₂O₃-CeO₂ supports with varying ratios (80Al/20Ce, 50Al/50Ce, 75Al/25Ce) were synthesized and evaluated for their catalytic performance in SMR. The mixed alumina-ceria supports were designed to combine the thermal stability of alumina with the oxygen storage capacity of ceria to enhance catalytic activity and resistance to carbon deposition. However, the results showed that the catalytic performance of mixed supports was lower compared to that of the Ni-Co-La catalyst supported solely on alumina.

Characterization studies revealed that the incorporation of ceria into the support matrix affected the metal dispersion and altered the interaction between active metal sites and the support. While ceria contributed to enhanced resistance against coking through its redox properties, it also led to larger particle sizes and reduced active surface area compared to the alumina-only support. Among the mixed supports, Ni-Co-La/80Al/20Ce exhibited the best performance due to its relatively higher dispersion and balanced metal-support interactions.

These findings suggest that while mixed Al₂O₃-CeO₂ supports offer advantages in terms of coking resistance, the catalytic activity in SMR is more effectively sustained with alumina-only supports due to their superior metal dispersion and stability. This study underscores the need for further optimization of mixed support systems to fully realize their potential in methane reforming reactions.

A1. Introduction

The choice of support material is a critical factor in influencing the catalytic performance, in addition to the metal composition. Although traditional alumina (Al_2O_3) supports have strong thermal stability and mechanical strength, they frequently have drawbacks such as weak metal-support interactions and low oxygen mobility. [1-2] In order to get over these restrictions, mixed support systems that combine ceria (CeO_2) and AlO_3 have been investigated. With its special ability to store and release oxygen, CeO_2 improves the catalyst's redox characteristics, assisting in the maintenance of a stable active phase and reducing coke deposition. [3-4] Combining CeO_2 and AlO_3 as supports can have a synergistic impact that enhances the overall performance of Ni-Co-La bimetallic catalysts in SMR by creating a highly effective environment. [5-10]

The synthesis, characterization, and catalytic testing of Ni-Co-La/ AlO_3 - CeO_2 catalysts for steam methane reforming are the main objectives of this work, which also focuses on the contribution of mixed supports to enhanced catalyst performance. The main goal is to investigate the effects of the AlO_3 - CeO_3 support system and the combination of Ni, Co, and La on the catalytic activity, coke resistance, and long-term stability. Well-known impregnation techniques will be used to create the catalysts, and a variety of characterization methods, including temperature-programmed reduction (TPR), scanning electron microscopy (SEM), transmission electron microscopy (TEM), and X-ray diffraction (XRD), will be used to assess their characteristics. These methods will shed light on the catalysts' electrical, morphological, and structural characteristics—all of which have a significant impact on how well they work. The catalytic behavior will be evaluated under typical SMR reaction conditions to assess the impact of the mixed support on activity, stability, and selectivity.

A2. Methodology

Table A1. Literature survey

Author	Title	Journal	Catalyst	Support	Key findings
AJ de Abreu et al, 2012 [6]	Ni catalyst on mixed support of CeO ₂ -ZrO ₂ and Al ₂ O ₃ : Effect of composition of CeO ₂ -ZrO ₂ solid solution on the methane steam reforming reaction	Fuel Processing Technology	Ni (Nickel)	CeO ₂ -ZrO ₂ , Al ₂ O ₃	Investigates the impact of CeO ₂ -ZrO ₂ composition on the performance of Ni-based catalysts in MSR, focusing on activity, stability, and the interaction with Al ₂ O ₃ support.
H Eltejaei, et al. 2012 [11]	Methane dry reforming on Ni/Ce _{0.75} Zr _{0.25} O ₂ -MgAl ₂ O ₄ and Ni/Ce _{0.75} Zr _{0.25} O ₂ - γ -alumina: effects of support composition and water addition	International Journal of Hydrogen Energy	Ni (Nickel)	Ce _{0.75} Zr _{0.25} O ₂ -MgAl ₂ O ₄ , Ce _{0.75} Zr _{0.25} O ₂ - γ -alumina	Focuses on the effects of support composition (Ce _{0.75} Zr _{0.25} O ₂ mixed with MgAl ₂ O ₄ or γ -alumina) on the performance of Ni catalysts for methane dry

					reforming, including the impact of water addition.
MS Aw et al., 2016 [12]	Transition metal pairs on ceria-promoted, ordered mesoporous alumina as catalysts for the CO ₂ reforming reaction of methane	Catalysis Science & Technology	Transition Metal Pairs (e.g., Ni, Co)	Ceria-promoted, ordered mesoporous alumina	Investigates the use of transition metal pairs on ceria-promoted mesoporous alumina supports for CO ₂ reforming of methane, focusing on catalytic activity and stability.
N Miletić et al. 2015 [13]	Oxidative steam reforming of methane over nickel catalysts supported on Al ₂ O ₃ -CeO ₂ -La ₂ O ₃	Catalysis Science & Technology	Ni (Nickel)	Al ₂ O ₃ -CeO ₂ -La ₂ O ₃	Studies the oxidative steam reforming of methane over Ni catalysts supported on a mixed oxide (Al ₂ O ₃ -CeO ₂ -La ₂ O ₃) system,

				focusing on catalytic performance and the role of support composition.
F Zarei-Jelyani et al. 2023 [14]	Response surface methodology for optimizing the activity of bimetallic Ni-Co-Ce/Al ₂ O ₃ catalysts in the steam methane reforming	Journal of the Energy Institute (Bimetallic)	Ni-Co-Ce Al ₂ O ₃	Utilizes response surface methodology (RSM) to optimize the activity of bimetallic Ni-Co-Ce catalysts supported on Al ₂ O ₃ for steam methane reforming, focusing on the effects of process parameters.

Several catalysts and supports for methane reforming processes are examined in this literature. Research focuses on how various support materials, including CeO₂-ZrO₂, Al₂O₃, and CeO₂-La₂O₃, affect the stability and activity of Ni-based catalysts. [15-19] The significance of support composition in improving catalytic performance for steam methane reforming, dry reforming, and oxidative reforming is highlighted by key discoveries.

Furthermore, bimetallic Ni–Co–Ce/Al₂O₃ catalysts for steam methane reforming were optimized using response surface methods, highlighting the impact of process variables on catalytic activity.

A3. Catalyst Preparation

A continuous tubular packed bed reactor with an internal diameter of 11.7 mm and a length of 60 cm was used to assess the catalyst activity. 0.769 grams of catalyst with a size range of 180–300 microns by mixing with same amount of inert was utilized throughout the entire experiment. Quartz particles of the same size were combined with the catalyst in a 1:1 ratio as inert. To get around the mass transfer restriction, the L/dp ratio was kept above 50 while the D/dp ratio was kept above 35. The catalyst was first reduced for two hours at 850 °C in an atmosphere containing 50% N₂ and 50% H₂ at a flow rate of 110 ml/min. After that, the reactor was kept at the appropriate operating temperature and flushed with pure nitrogen for an hour to remove all of the hydrogen.

Nitrogen and a combination of methane and water were added to the reactor when the temperature was stabilized and no hydrogen was found at the reactor's outflow. All experiments were conducted with a methane to steam ratio of 1: 4. At a W/F of 26.8 kg_{cat}.s/mol and a gas hourly space velocity (GHSV) of 10,739 hr⁻¹, the experiments were conducted. The liquid product was condensed by passing the output gas through a condenser and gas-liquid separator. A TCD-equipped GC (Nucon GC) was then used to evaluate the output gases utilizing a parallel column system of Porapak Q (1 m length, I.D. 2 mm) and Molecular sieve (3 m length, I.D 2 mm). The CO selectivity, CO₂ selectivity, and CH₄ conversion were computed using the following formulas.

A4. Catalyst Characterization

Certain catalysts were analyzed using a Transmission electron microscope (TEM), scanning electron microscope (SEM), and in order to determine their physical and chemical properties.

The Tecnai G2 20 TWIN equipment is used for TEM investigation in order to scan the surface morphology of catalysts. A pinch of catalyst is suspended in ethanol and allowed to sonicate for at least 30 minutes in order to create the TEM sample. Following that, a single drop of the suspended solution is applied to the TEM copper grid's surface and allowed to dry for a full day. To determine the alteration in surface morphology following the reaction, TEM analysis is also performed on the wasted catalysts.

In order to identify the elements, the surface morphology and properties of selected sample sections were analyzed using an X-ray energy dispersive spectroscopy (EDS) system and a SEM (Nova Nano SEM 450). Using EDS mapping, the elemental composition was also determined. The measurement indices for the SEM images varied from 5 μm to 500 μm . N_2 adsorption desorption at 77 K (liquid nitrogen temperature) is used to assess the textural qualities utilizing the BET and BJH desorption techniques on (Meso 112) equipment in order to determine the surface and pore parameters. Using a BET surface analyzer, the catalysts' surface area and pore size distribution were examined. The samples were vacuum degassed for two hours at 200 °C to eliminate adsorption species before analysis.

A5. Catalyst Activity

In current work, trimetallic catalysts supported on mixed supports alumina and ceria are synthesized for hydrogen generation using steam methane reforming that consists of a prefixed ratio of metals Ni, Co and La loaded . All precursors salts supplied by Merck Chemicals. Alumina and ceria is used as a support material. The total metal loading is

varied from 5 to 15wt.%. Nickel ratio is 75wt%, Co:La ratio is 20:5 wt.% of the total metal loading.

First of all, gamma alumina in powder form as a support is calcined in a muffle furnace at 970°C temperatures at a rate of 1°C/minute for 6 hours time to obtain the powder of theta alumina as catalyst support. Then theta alumina support is mixed with the ceria support using dry impregnation method. In this method, amount of distilled water is used as equal to the pore diameter of theta alumina as represented in the BET table. Cerium (III) nitrate hexahydrate is dissolved in this amount of distilled water and properly mixed. Then solid powder is kept in oven for overnight at temperature 120°C. Then dried powder is calcined in muffle furnace at 970°C. The prepared support is mixed Ce-Al₂O₃.

Nickel nitrate hexahydrate is used as a precursor salt for nickel whereas, cobalt nitrate nonahydrate and Lanthanum nitrate hexahydrate are used as precursor for cobalt and lanthanum metal loading respectively. All precursors are added into mixed support solution with vigorous stirring at temperature 70°C. This solution is kept for 10 hours of time under vigorous stirring in a trimetallic mixture solution. The pH is maintained between 6-8 to obtain a slurry, and then this obtained slurry is kept for drying at 120°C temperature for overnight. This is followed by crushing and calcination to turn the nitrates into oxides in the presence of air at 970°C temperature for 6 hours in a muffle furnace to obtain a trimetallic catalyst. Then this calcinated catalyst is crushed in a mortar pestle to get the desired size of 180-300 microns. The same is used for characterization and testing.

A6. Results and discussion

Activity Results

Effect of Alumina/Ceria ratio on conversion

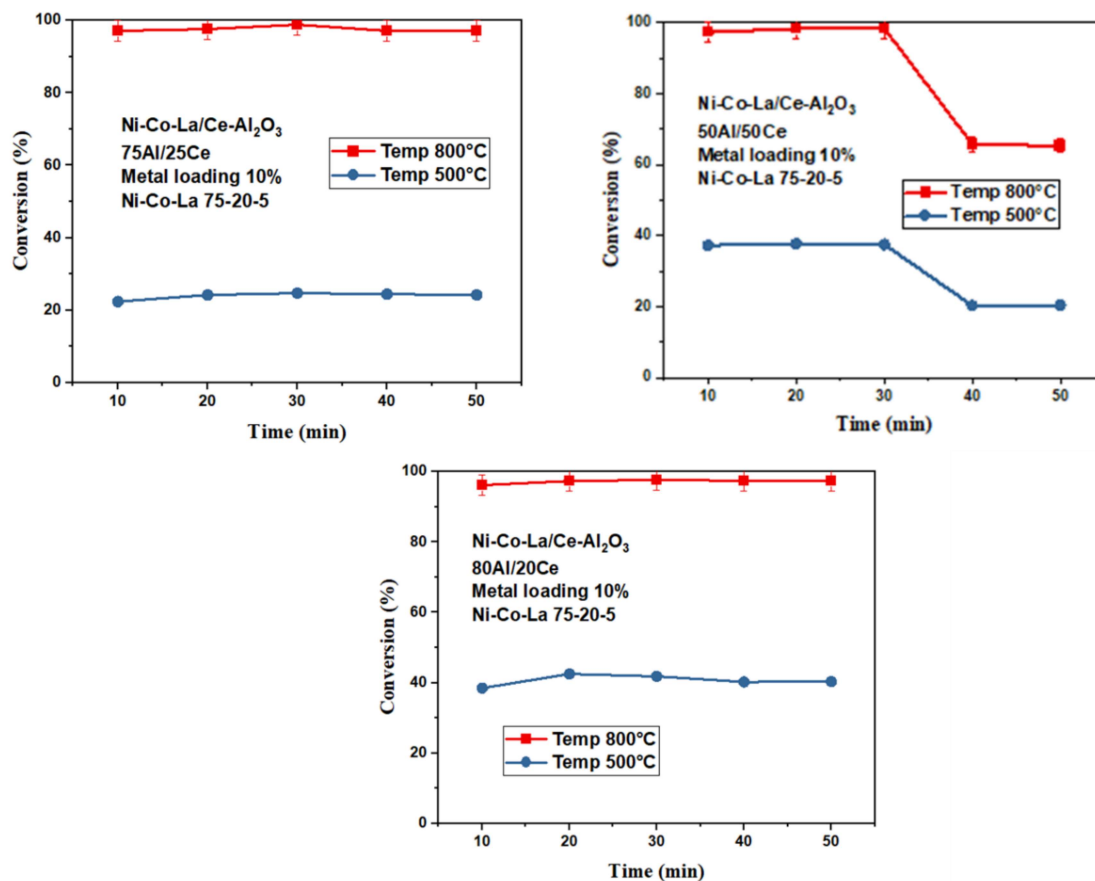


Fig. A1. Conversion vs time graph (a) 75Al/25Ce (b) 50Al/50Ce (c) 80Al/20Ce

When steam methane reforming is carried out using a Ni-Co-La catalyst on mixed supports of alumina (Al₂O₃) and ceria (CeO₂) at two temperatures, 500°C and 800°C. The graphs show the methane conversion with time for 75% alumina/25% ceria, 50% alumina/50% ceria, and 80% alumina/20% ceria are the three support compositions that are examined as represented in Fig 1. In contrast to 500°C, all compositions show noticeably increased methane conversion at 800°C, demonstrating the improved reaction kinetics at higher temperatures. [20-22]

At 800°C, the 80% alumina/20% ceria composition of the supports achieves the highest and most stable conversion, suggesting that the redox characteristics of ceria and the structural stability of alumina work in perfect harmony. At 800°C, the 75% alumina/25% ceria support likewise functions effectively, sustaining constant conversion over time. Conversely, the 50% alumina/50% ceria composition exhibits decreasing conversion at 800°C, indicating possible catalyst deactivation brought on by a lack of alumina to sustain carbon removal and redox cycles. All supports exhibit decreased conversion at 500°C, with the 80% alumina/20% ceria composition once more exhibiting the best consistent performance. At this temperature, the 50% alumina/50% ceria support exhibits the lowest conversion, with a discernible decrease with time, suggesting that this ratio is not ideal for low-temperature reforming. Overall, the 80% alumina/20% ceria support emerges as the most effective composition, offering the best balance of catalytic activity and stability, particularly at high temperatures.

Temperature effect for the 80Al/20Ce ratio

The graph illustrates the relationship between methane conversion and reaction time during steam methane reforming at four different temperatures: 500°C, 600°C, 700°C, and 800°C. At higher temperatures (700°C and 800°C), the methane conversion remains consistently high and stable over time, indicating favorable reaction kinetics and minimal catalyst deactivation. In contrast, at 600°C, the conversion starts high but decreases slightly over time, suggesting some degree of catalyst deactivation or reaction inefficiency. At 500°C, the conversion is significantly lower and exhibits a gradual decline over time, which could be attributed to the slower reaction rates and increased susceptibility to low conversion at lower temperatures.

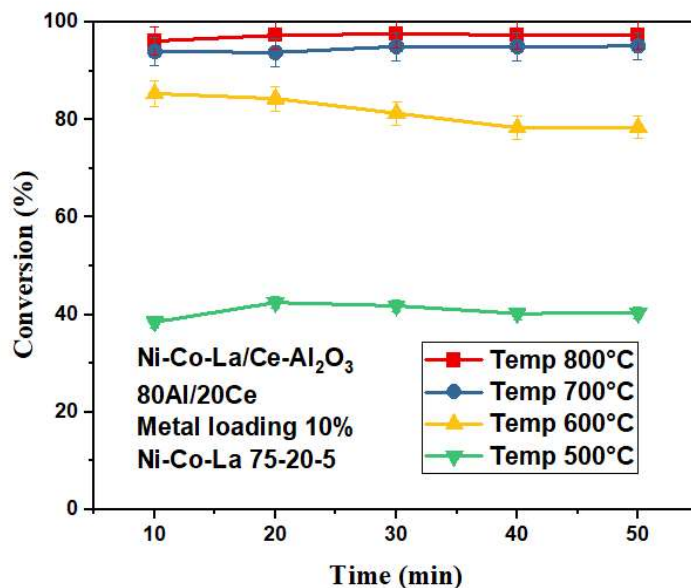


Fig. A2. Conversion vs time graph of 80Al/20Ce ratio for all temperatures

These trends emphasize the importance of maintaining a high reaction temperature to achieve optimal methane conversion and sustain catalyst activity during steam reforming.

CO selectivity and CO₂ selectivity

The graph depicts the CO selectivity (left) and CO₂ selectivity (right) during steam methane reforming at different temperatures (500°C, 600°C, 700°C, and 800°C) over time. At 700°C, CO₂ selectivity remains low and stable, while CO selectivity is consistently high, reflecting favorable conditions for complete methane reforming and water-gas shift reactions. At 800°C, a similar trend is observed, though with slightly higher CO selectivity and marginally lower CO₂ selectivity compared to 700°C. At 600°C, CO₂ selectivity is higher than at 700°C and shows a slight decrease over time, while CO selectivity is stable but slightly increased, indicating incomplete conversion or reduced efficiency of the water-gas shift reaction.

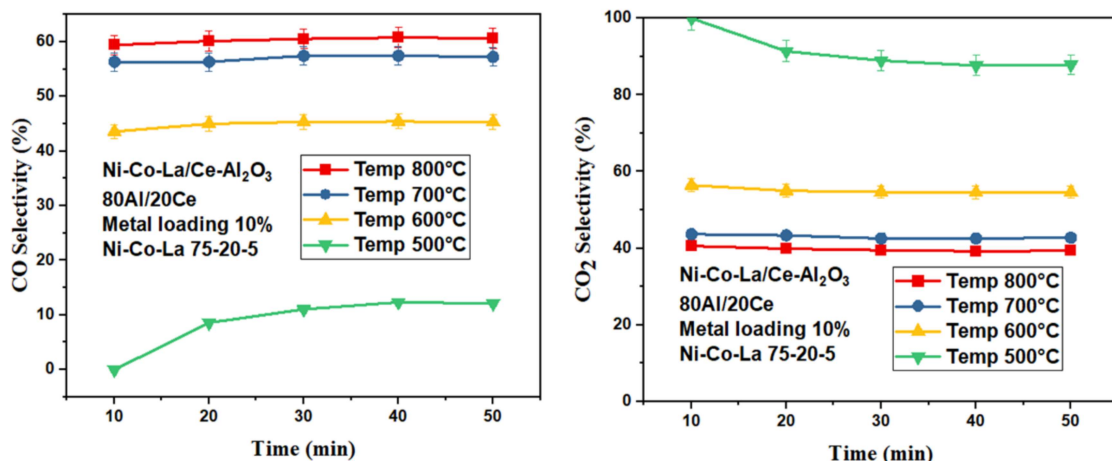


Fig. A3. (a) CO selectivity vs time graph of 80Al/20Ce catalyst (b) CO₂ selectivity vs time graph

At 500°C, CO₂ selectivity is significantly higher and decreases over time, while CO selectivity is lower and increases, suggesting inefficient reforming and a low tendency for carbon monoxide formation due to limited reaction kinetics. These trends emphasize the importance of low temperatures (500°C and 600°C) for achieving optimal CO₂ selectivity and minimizing CO selectivity, which is crucial for efficient hydrogen production and reduced carbon monoxide levels.

A7. Comparative analysis of mixed support with only alumina

Effect of Conversion

The graph as represented in Fig 5 shows the methane conversion over time during steam reforming using Ni-Co-La/Ce-Al₂O₃ (80Al/20Ce) and Ni-Co-La/Al₂O₃ catalysts at 800°C and 500°C. At 800°C, the Ni-Co-La/Al₂O₃ catalyst exhibits near-complete and stable methane conversion, outperforming Ni-Co-La/Ce-Al₂O₃. Although incorporation of CeO₂, which enhances the catalyst's oxygen storage capacity, redox behavior, and active metal dispersion but there is no such effect observed with the mixed support for conversion. At 500°C, both catalysts show reduced conversion due to slower reaction kinetics, but the Ni-

Co-La/Al₂O₃ catalyst still maintains higher conversion compared to Ni-Co-La/Ce-Al₂O₃. The stability of methane conversion over time, especially at 800°C, indicates excellent thermal stability for both catalysts under high-temperature conditions. The results demonstrate that the addition of CeO₂ as a mixed support not improved catalytic performance for this ratio and with this preparation method.

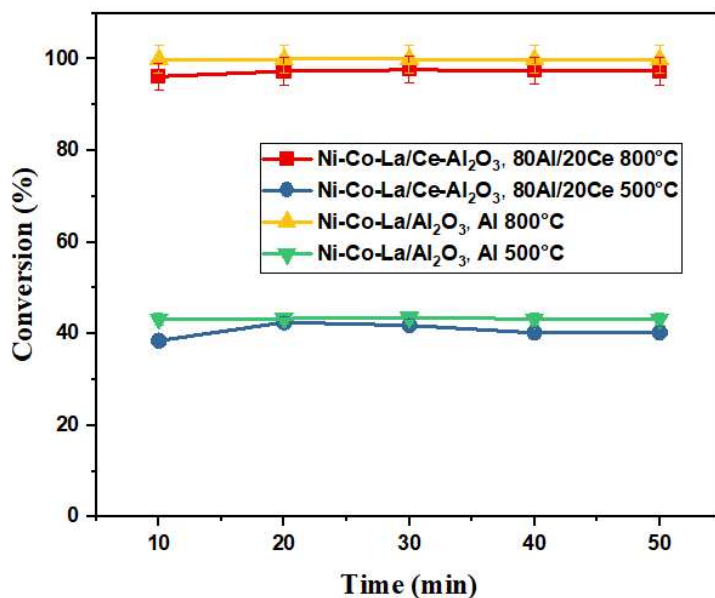


Fig. A4. Conversion vs time graph of mixed support and without ceria support

Effect of CO and CO₂ selectivity

The graphs illustrate CO selectivity (left) and CO₂ selectivity (right) over time during steam methane reforming for different catalysts: Ni-Co-La/Ce-Al₂O₃ (80Al/20Ce) and Ni-Co-La/Al₂O₃ at 800°C and 500°C. For CO selectivity, the Ni-Co-La/Al₂O₃ catalyst at 800°C shows consistently low and stable values, indicating efficient conversion of CO to CO₂ via the water-gas shift reaction. At 500°C, CO selectivity for Ni-Co-La/Ce-Al₂O₃ catalyst starts slightly higher but decreases over time, reflecting slower reaction kinetics at lower temperatures.[23-25] The Ni-Co-La/Ce-Al₂O₃ catalyst at both temperatures exhibits higher CO selectivity, especially at 500°C, suggesting less efficient CO₂ formation and potential limitations in the water-gas shift reaction.

In the CO₂ selectivity graph, the Ni-Co-La/Al₂O₃ catalyst at 500°C demonstrates the highest and most stable CO₂ selectivity, confirming its superior performance in converting methane to H₂ while minimizing CO formation. At 500°C, CO₂ selectivity for this catalyst is high and shows a stable trend. In contrast, Ni-Co-La/Ce-Al₂O₃ at both temperatures displays significantly lower CO₂ selectivity, particularly at 800°C, where the values decrease over time, potentially due to catalyst deactivation or incomplete reaction pathways. Overall, these results highlight the enhanced catalytic efficiency of Ni-Co-La/Al₂O₃ (80Al/20Ce), due to active site availability provided by the Al₂O₃ support.

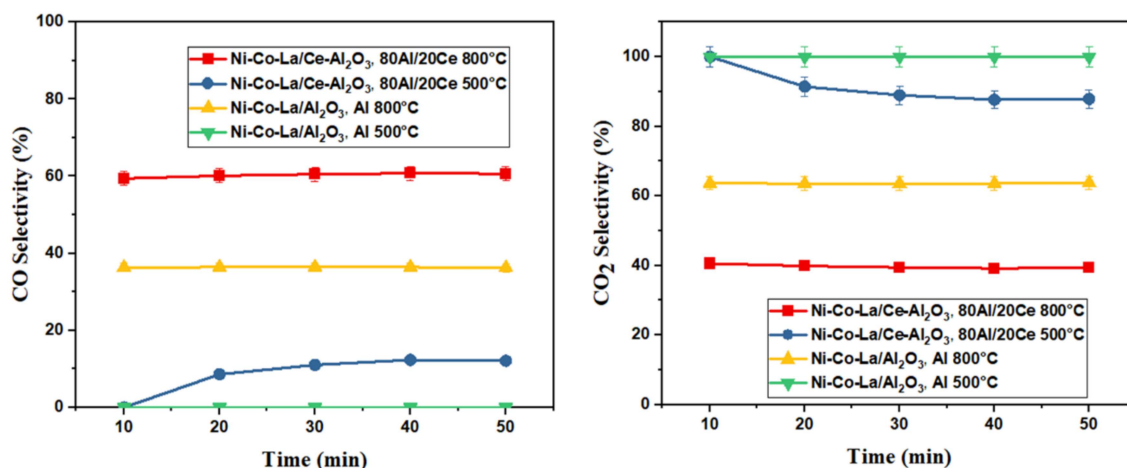


Fig. A5. (a) CO selectivity vs time graph (b) CO₂ selectivity vs time graph

Effect of W/F on reaction activity

The methane conversion, CO selectivity, and hydrogen yield at different weight flow rates (W/F) are represented in the graphs, which show the catalyst performance over time in steam methane reforming. The first graph, which illustrates the conversion of methane, shows that while lower W/F values, like 17 kg_{cat}·s/mol, result in reduced conversion, highlighting the significance of adequate catalyst contact time, higher W/F values, like 31

kg_{cat}·s/mol, consistently achieve high conversion rates, indicating efficient reforming. [27-29]

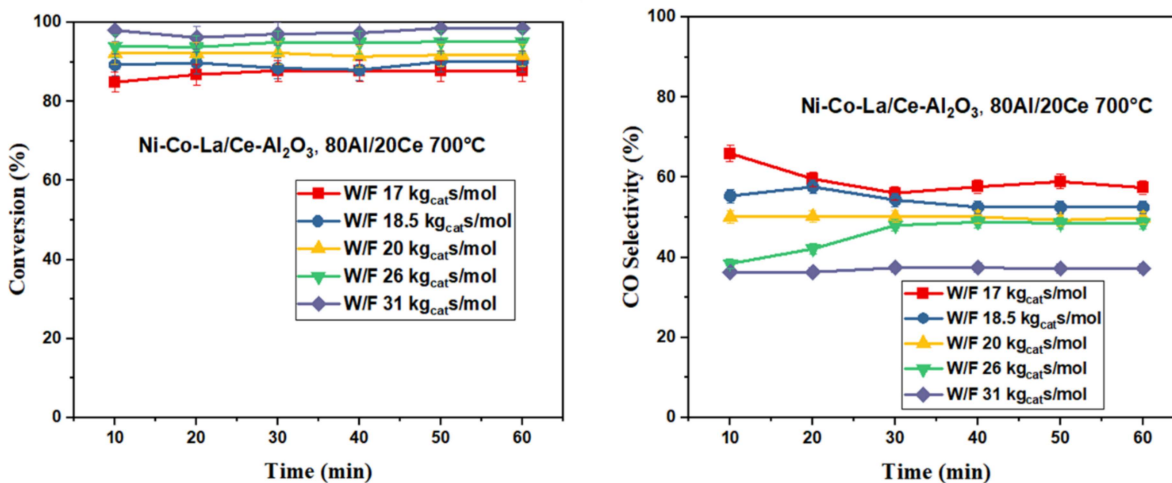


Fig. A6. Effect of W/F for Ni-Co-La/Ce-Al₂O₃ catalyst

Lower W/F ratios show stronger CO selectivity, as shown in the second graph, which shows CO selectivity. This is probably because of side reactions or incomplete methane conversion. Increasing the W/F, on the other hand, decreases CO selectivity, promoting hydrogen generation and reducing CO as a byproduct. The third graph, which displays hydrogen yield, shows that while lower W/F values result in lower yields because of limited methane conversion and increased CO production, higher W/F values continuously produce higher hydrogen yields over time. With maximal methane conversion, low CO selectivity, the catalyst functions best overall at higher W/F values, highlighting the significance of W/F optimization for effective hydrogen production.

A8. Characterization results

SEM

The SEM images labeled (a), (b), and (c) show the surface morphology of the Ni-Co-La catalysts supported on CeO₂-Al₂O₃ with varying compositions of ceria and alumina. These images provide insights into the dispersion, particle size, and surface texture of the

catalysts, which are critical parameters for their performance in steam methane reforming (SMR).[30-31]

- **75Al/25Ce:** This composition seems to exhibit relatively larger particles with a rough surface texture. The aggregates are loosely packed, which may indicate a lower degree of ceria dispersion on the alumina surface. This could lead to fewer active sites being available for SMR.
- **80Al/20Ce:** The particles in this composition appear to be more homogeneously distributed, with a denser and more uniform texture. This suggests improved interaction between ceria and alumina, enhancing the catalyst stability and providing a larger active surface area for SMR.
- **50Al/50Ce:** This composition shows finer particles and a relatively smooth surface compared to the other images. The uniformity in particle size indicates a high degree of ceria dispersion, which is beneficial for catalyst activity. However, excessive ceria content may hinder optimal alumina interactions, potentially affecting catalyst performance.

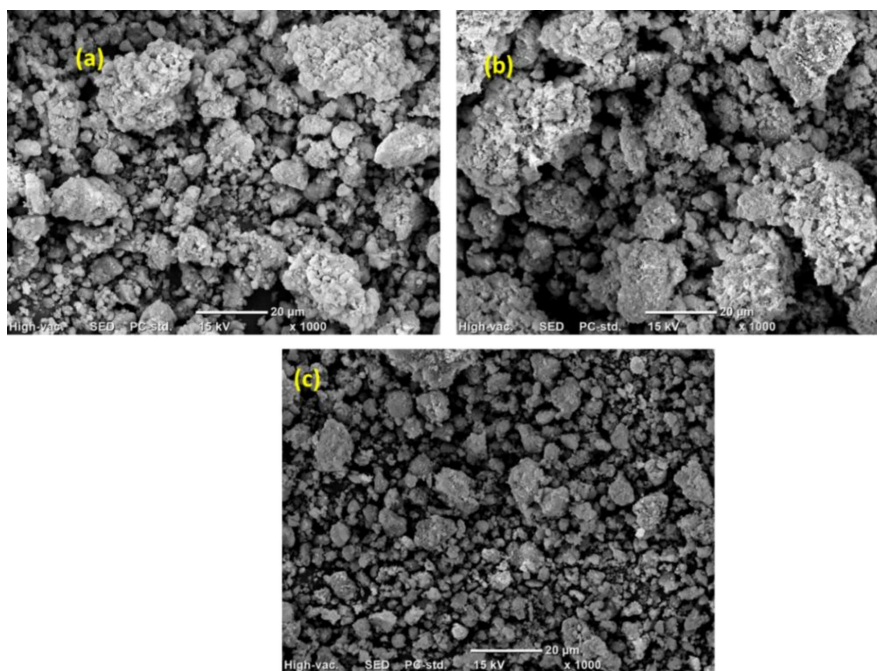


Fig. A7. SEM images of (a)75Al/25Ce (b) 80Al/20Ce (c) 50Al/50Ce

In summary, these SEM images reveal how the variation in ceria and alumina compositions influences the morphological features of the catalysts. The balance between ceria and alumina is crucial to optimize the active surface area, particle dispersion, and thermal stability, all of which are key to achieving high efficiency in steam methane reforming.

TEM

The TEM images provided depict the morphology of catalysts prepared with varying ratios of Al_2O_3 (alumina) and CeO_2 (ceria) as support materials for steam methane reforming. The images on the left show the nanoscale dispersion of catalyst particles, while the corresponding SAED (Selected Area Electron Diffraction) patterns in the middle reveal the crystalline nature of the materials. The histograms on the right illustrate the particle size distributions, highlighting the average particle sizes for each catalyst formulation. [32-33] 80Al/20Ce sample, likely with a higher alumina content, shows a relatively fine dispersion of particles with an average particle size concentrated around 10–12 nm. The SAED pattern indicates well-defined diffraction rings, suggesting a polycrystalline structure.

75Al/25Ce: In this sample, with a more balanced alumina-to-ceria ratio, the particle distribution appears slightly broader, with an average particle size of approximately 15–18 nm. The SAED pattern retains clear diffraction rings, indicating good crystallinity while potentially reflecting an intermediate phase contribution from both alumina and ceria. 50Al/50Ce catalyst, likely with a higher ceria content, displays a further increase in particle size, averaging around 20–25 nm, as reflected in the histogram. The SAED pattern shows slightly more intense diffraction rings, indicative of increased ceria crystallinity and potentially reduced alumina dispersion.

The results demonstrate that the alumina-to-ceria ratio significantly influences the particle size and dispersion, which are crucial parameters for catalytic activity in steam methane

reforming. Smaller, well-dispersed particles with balanced crystalline features generally enhance the catalyst's active surface area and stability.

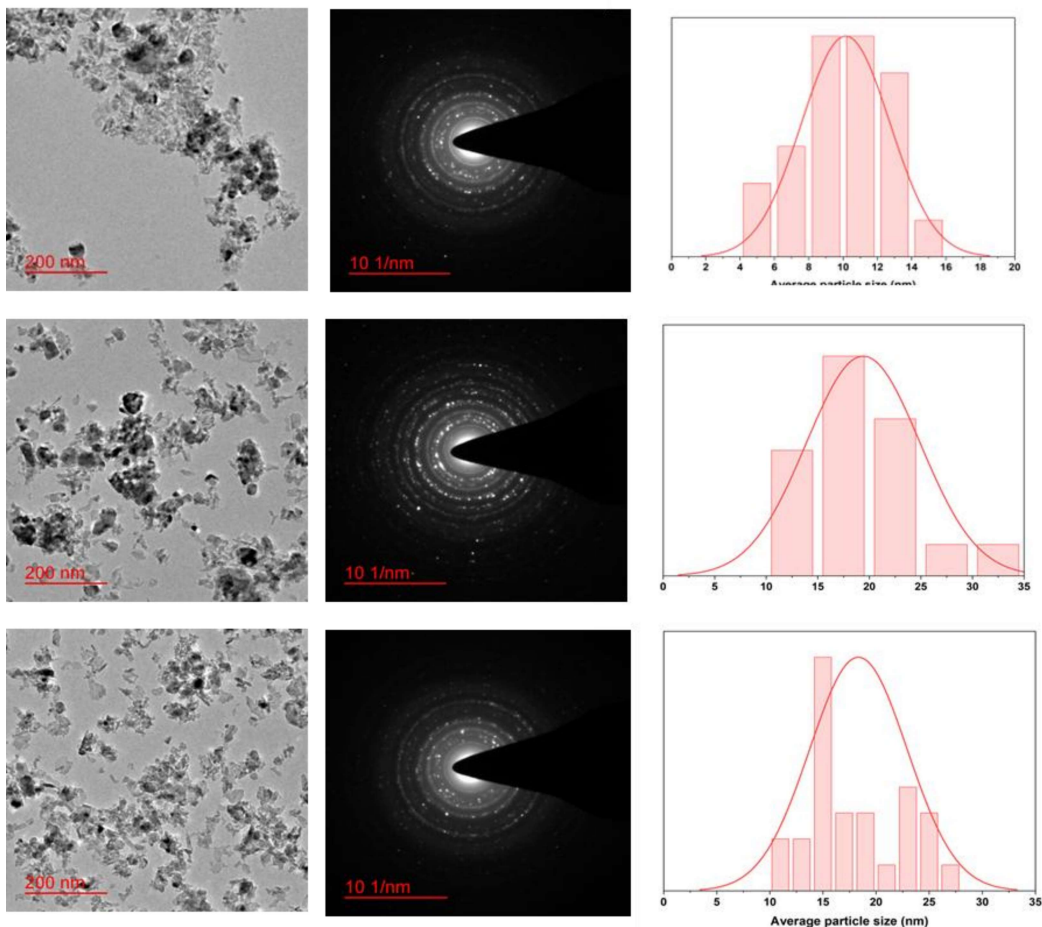


Fig. A8. TEM images of mixed supports(a) 80Al/20Ce (b) 75Al/25Ce (c) 50Al/50Ce

A9. Conclusions

This study examined the effects of mixed alumina-ceria supports with different ratios (80Al/20Ce, 50Al/50Ce, and 75Al/25Ce) on the catalytic performance of Ni-Co-La catalysts in steam methane reforming. Particle size, dispersion, and crystalline features are among the properties of the catalyst that are mostly determined by the alumina-ceria ratio, according to structural, morphological, and catalytic activity assessments. The Ni-Co-La/80Al/20Ce catalyst performed the best overall out of all the compositions that were examined.

Ni-Co-La/80Al/20Ce greater activity is due to its optimized support qualities, which allow better dispersion of active metal species, increased surface area, and improved metal-support interactions. The larger alumina concentration in the 80Al/20Ce ratio improved thermal stability and dispersion, while the ceria component increased oxygen storage capacity and facilitated carbon deposit removal, lowering the possibility of catalyst deactivation.

Thus, the Ni-Co-La/80Al/20Ce catalyst proved to be the most effective formulation for steam methane reforming, due to its high activity, stability, and resistance to coking. These findings emphasize the need of adjusting the alumina-ceria ratio in mixed supports to improve catalyst performance and provide useful insights for the design of advanced reforming catalysts. But for this study, catalytic activity of mixed supports is less as compared to the only alumina. These results conclude that mixed support is not effective strategy for steam methane reforming at these operating conditions.

References

1. Arcotumapathy, V., Vo, D. V. N., Chesterfield, D., Tin, C. T., Siahvashi, A., Lucien, F. P., Adesina, A. A. (2014). Catalyst design for methane steam reforming. *Applied Catalysis A: General*, 479, 87-102.
2. Jimenez-Gonzalez, C., Boukha, Z., de Rivas, B., Gonzalez-Velasco, J. R., Gutierrez-Ortiz, J. I., López-Fonseca, R. (2014). Behavior of coprecipitated NiAl₂O₄/Al₂O₃ catalysts for low-temperature methane steam reforming. *Energy & fuels*, 28(11), 7109-7121.
3. Xu, J., Yeung, C. M., Ni, J., Meunier, F., Acerbi, N., Fowles, M., Tsang, S. C. (2008). Methane steam reforming for hydrogen production using low water-ratios without carbon formation over ceria coated Ni catalysts. *Applied Catalysis A: General*, 345(2), 119-127.
4. Iglesias, I., Forti, M., Baronetti, G., Mariño, F. (2019). Zr-enhanced stability of ceria based supports for methane steam reforming at severe reaction conditions. *International Journal of Hydrogen Energy*, 44(16), 8121-8132.
5. Demsash, H. D., Mohan, R. (2016). Steam reforming of glycerol to hydrogen over ceria promoted nickel–alumina catalysts. *International journal of hydrogen energy*, 41(48), 22732-22742.
6. de Abreu, A. J., Lucrédio, A. F., Assaf, E. M. (2012). Ni catalyst on mixed support of CeO₂–ZrO₂ and Al₂O₃: Effect of composition of CeO₂–ZrO₂ solid solution on the methane steam reforming reaction. *Fuel Processing Technology*, 102, 140-145.
7. Aouad, S., Gennequin, C., Mrad, M., Tidahy, H. L., Estephane, J., Aboukaïs, A., Abi-Aad, E. (2016). Steam reforming of methanol over ruthenium impregnated ceria, alumina and ceria–alumina catalysts. *International Journal of Energy Research*, 40(9), 1287-1292.

8. Palma, V., Meloni, E., Renda, S., Martino, M. (2020). Catalysts for methane steam reforming reaction: evaluation of CeO₂ addition to alumina-based washcoat slurry formulation. *C*, 6(3), 52.
9. Iriondo, A., Barrio, V. L., Cambra, J. F., Arias, P. L., Guemez, M. B., Sanchez-Sanchez, M. C., Fierro, J. L. G. (2010). Glycerol steam reforming over Ni catalysts supported on ceria and ceria-promoted alumina. *International journal of hydrogen energy*, 35(20), 11622-11633.
10. Lai, G. H., Lak, J. H., Tsai, D. H. (2019). Hydrogen production via low-temperature steam–methane reforming using Ni–CeO₂–Al₂O₃ hybrid nanoparticle clusters as catalysts. *ACS Applied Energy Materials*, 2(11), 7963-7971.
11. Eltejaei, H., Bozorgzadeh, H. R., Towfighi, J., Omidkhah, M. R., Rezaei, M., Zanganeh, R., Ghalam, A. Z. (2012). Methane dry reforming on Ni/Ce_{0.75}Zr_{0.25}O₂–MgAl₂O₄ and Ni/CeO₂–γ-alumina: effects of support composition and water addition. *International journal of hydrogen energy*, 37(5), 4107-4118.
12. Aw, M. S., Dražić, G., Djinović, P., Pintar, A. (2016). Transition metal pairs on ceria-promoted, ordered mesoporous alumina as catalysts for the CO₂ reforming reaction of methane. *Catalysis Science & Technology*, 6(11), 3797-3805.
13. Miletić, N., Izquierdo, U., Obregón, I., Bizkarra, K., Agirrezabal-Telleria, I., Barrio, L. V., Arias, P. L. (2015). Oxidative steam reforming of methane over nickel catalysts supported on Al₂O₃–CeO₂–La₂O₃. *Catalysis Science & Technology*, 5(3), 1704-1715.
14. Zarei-Jelyani, F., Salahi, F., Meshksar, M., Farsi, M., Rahimpour, M. R. (2023). Response surface methodology for optimizing the activity of bimetallic Ni–Co–Ce/Al₂O₃ catalysts in the steam methane reforming. *Journal of the Energy Institute*, 110, 101363.

15. Pereira, V. G. F., Serrano-Lotina, A., Portela, R., Bañares, M. A., Rodrigues, C. P., Toniolo, F. S. (2025). Ni/Al₂O₃ promoted by CeO₂, CeO₂-La₂O₃, and CeO₂-ZrO₂ supported on cordierite monoliths for methane steam reforming. *Catalysis Today*, 445, 115107.
16. Isarapakdeetham, S. (2018). Effect of CeO₂ and La₂O₃ promoters on Ni/Al₂O₃ oxygen carrier performance in chemical looping steam reforming of ethanol for hydrogen production.
17. Braga, A. (2024). Preparation and characterisation of bimetallic catalysts for the steam reforming of methane.
18. Razzaq, R. (2022). Effect of Neodymium on the development of Ni supported catalysts for carbon dioxide reforming of methane.
19. Abreu, A. J. D. Development and characterization of nickel catalysts supported in CeO₂-ZrO₂-Al₂O₃, CeO₂-La₂O₃-Al₂O₃, ZrO₂-La₂O₃-Al₂O₃ matrixes evaluated for methane reforming reactions.
20. Matsumura, Y., Nakamori, T. (2004). Steam reforming of methane over nickel catalysts at low reaction temperature. *Applied Catalysis A: General*, 258(1), 107-114.
21. Dupont, V., Ross, A. B., Knight, E., Hanley, I., Twigg, M. V. (2008). Production of hydrogen by unmixed steam reforming of methane. *Chemical Engineering Science*, 63(11), 2966-2979.
22. Halabi, M. H., De Croon, M. H. J. M., Van der Schaaf, J., Cobden, P. D., Schouten, J. C. (2010). Low temperature catalytic methane steam reforming over ceria–zirconia supported rhodium. *Applied Catalysis A: General*, 389(1-2), 68-79.
23. Nieva, M. A., Villaverde, M. M., Monzón, A., Garetto, T. F., Marchi, A. J. (2014). Steam-methane reforming at low temperature on nickel-based catalysts. *Chemical Engineering Journal*, 235, 158-166.

24. Roh, H. S., Wang, Y., King, D. L., Platon, A., Chin, Y. H. (2006). Low temperature and H₂ selective catalysts for ethanol steam reforming. *Catalysis letters*, 108, 15-19.
25. Kusakabe, K., Sotowa, K. I., Eda, T., Iwamoto, Y. (2004). Methane steam reforming over Ce–ZrO₂ supported noble metal catalysts at low temperature. *Fuel Processing Technology*, 86(3), 319-326.
26. Contreras, J. L., Salmones, J., Colín-Luna, J. A., Nuño, L., Quintana, B., Córdova, I., Fuentes, G. A. (2014). Catalysts for H₂ production using the ethanol steam reforming (a review). *International Journal of Hydrogen Energy*, 39(33), 18835-18853.
27. Byun, M., Lee, B., Lee, H., Jung, S., Ji, H., Lim, H. (2020). Techno-economic and environmental assessment of methanol steam reforming for H₂ production at various scales. *International Journal of Hydrogen Energy*, 45(46), 24146-24158.
28. Hou, K., Hughes, R. (2001). The kinetics of methane steam reforming over a Ni/ α -Al₂O₃ catalyst. *Chemical Engineering Journal*, 82(1-3), 311-328.
29. Naseri, A. T., Peppley, B. A., Pharoah, J. G. (2015). A systematic parametric study on the effect of a catalyst coating microstructure on its performance in methane steam reforming. *International Journal of Hydrogen Energy*, 40(46), 16086-16095.
30. Lai, G. H., Lak, J. H., Tsai, D. H. (2019). Hydrogen production via low-temperature steam–methane reforming using Ni–CeO₂– Al₂O₃ hybrid nanoparticle clusters as catalysts. *ACS Applied Energy Materials*, 2(11), 7963-7971.
31. Bozdağ, A. A., Sezgi, N. A., Doğu, T. (2022). Effects of synthesis route on the performance of mesoporous ceria-alumina and ceria-zirconia-alumina supported nickel catalysts in steam and autothermal reforming of diesel. *International Journal of Hydrogen Energy*, 47(7), 4568-4583.
32. Duarte, R. B., Safonova, O. V., Krumeich, F., Makosch, M., van Bokhoven, J. A. (2013). Oxidation state of Ce in CeO₂-promoted Rh/Al₂O₃ catalysts during methane

steam reforming: H₂O activation and alumina stabilization. *ACS Catalysis*, 3(9), 1956-1964.

33. Zhang, Z., Wei, T., Chen, G., Li, C., Dong, D., Wu, W., Hu, X. (2019). Understanding correlation of the interaction between nickel and alumina with the catalytic behaviors in steam reforming and methanation. *Fuel*, 250, 176-193.